Neutron field of accelerator-driven p(35 MeV)+Be fast neutron source at NPI Rez

Milan Stefanik[1,2,a], Pavel Bem[1], Mitja Majerle[1], Jan Novak[1], and Eva Simeckova[1]

[1] Nuclear Physics Institute of The Czech Academy of Sciences p.r.i., Rez No. 130, 250 68 Rez, Czech Republic

[2] Czech Technical University in Prague, Faculty of Nuclear Sciences and Physical Engineering, Brehova 7, 115 19 Prague, Czech Republic

Abstract. The accelerator driven fast neutron sources of the white- and quasi-monoenergetic spectra are operated at the NPI Rez Fast Neutron Facility utilizing the Be(thick), D_2O(thick), and ^{7}Li(C) target stations and the variable energy proton beam (up to 37 MeV) from the U-120M isochronous cyclotron. Recently, the design of beryllium target station was upgraded in order to provide the higher neutron flux at the modified positions of irradiated samples. Afterwards, the thick target neutron field of the p+Be source reaction was investigated for proton energy of 35 MeV. The spectral neutron flux for several target-to-sample distances was determined using the multi-foil activation technique. From measured reaction rates, new neutron spectra were reconstructed employing the SAND-II unfolding code and validated against the MCNPX predictions. The IFMIF-like (International Fusion Material Irradiation Facility) neutron field obtained from the p(35)+Be source is suitable for the neutron cross-sections validation within the IFMIF research program, radiation hardness tests of electronics, and neutron activation analysis experiments.

1. Introduction

The accelerator-driven neutron sources represent the appropriate devices for neutron field production of precisely given parameters that are useful for clinical neutron radiotherapy, measurement and validation of nuclear data for advanced nuclear energetic applications, and for material hardness study. The Nuclear Physics Institute of the CAS belongs to laboratories that operate such types of cyclotron based fast neutron generators.

2. Materials and methods

2.1. The p + Be neutron source reaction

The accelerator-driven fast neutron generators with broad neutron spectrum are mostly built on the thick beryllium targets. High value of beryllium melting point (1287°C [1]) makes possible to use the intensive proton beams and thus to obtain higher neutron yield.

During the proton bombardment of beryllium target, the high energy neutron spectrum component is produced by the ^{9}Be(p,n)^{9}B reaction; the low energy spectrum fraction is formed in the multi-body break-up processes (see Table 1).

The p+Be source reaction was intensively studied by several scientists in the 70s and 80s years of the last century. Neutron spectra were investigated by M.A. Lone [3], R.G. Graves [4], H.J. Brede [5], S.W. Johnsen [6], W.B. Howard [7], F.M. Waterman [8], and J.L. Ullman [9]. For thick Be-target it was found that the fluence-averaged energy of neutrons above 2 MeV emitted at an angle of 0 °C an be estimated from the empirical equation [3,10]:

$$\bar{E}_n = 0.47 \times E_p - 2.2, \tag{1}$$

where E_p is the proton beam energy. For 35 MeV proton beam, the average energy of neutron spectrum above 2 MeV should be 14.2 MeV.

2.2. Beryllium target station NG-2 at NPI

The beryllium target station NG-2 (see Fig. 1) of the NPI CAS has been in standard operation with 35 MeV proton beam since 2012 [11]. In order to obtain the higher neutron flux for sample irradiation (e.g. for radiation hardness tests of electronic devices and materials related to the IFMIF research program [12]), the Be-target head was recently rebuilt. Within the upgrade, the amount of construction materials in the area of target was reduced. It enabled also to modify the irradiation positions and put investigated samples close to the production target.

The Be-target station of NG-2 neutron generator (Fig. 1) is operated in the negative ion-mode of acceleration employing the 35 MeV proton beam from the U-120M isochronous cyclotron with intensities up to 15 μA (power of 525 W). The alcohol cooled static Be-target has a diameter of 50 mm and thickness of 8 mm.

Neutron spectra for two irradiation positions of the original version of Be-target station with the p(35)+Be reaction were reported for the first time in [11], and spectral characteristics were analysed in [13] in detail.

2.3. Multi-foil activation technique, reaction rate

The multi-foil activation technique allows determination of the neutron spectrum from the set of experimentally

[a] e-mail: `milan.stefanik@fjfi.cvut.cz`

Table 1. Proton induced reactions on beryllium target [2].

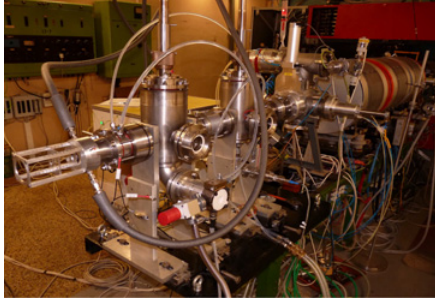| Reaction	(p,n)	(p,pn)	(p,pα)	(p,nα)	(p,pnα)
Product	^{9}B	^{8}Be	^{5}He*	^{5}Li	^{4}He
Q (MeV)	−1.85	−1.66	−2.31	−3.54	−1.57
E_{th} (MeV)	2.06	1.85	2.57	3.93	1.75

Figure 1. Beryllium target station NG-2 with aluminium holder of activation foils after modification of target station head.

measured reaction rates utilizing the unfolding code (e.g. SAND-II). The reaction rate per one target nuclei is obtained from the gamma-ray spectrometry measurements using the equation:

$$R_R = \frac{S\left(E_\gamma\right) \lambda \frac{t_{real}}{t_{live}}}{N_0 \left(1 - e^{-\lambda t_{irr}}\right) e^{-\lambda t_{cool}} \left(1 - e^{-\lambda t_{real}}\right) \varepsilon^\gamma_{FEP}(E_\gamma)\, I_\gamma(E_\gamma)} \quad (2)$$

where λ is the decay constant of produced radionuclide, S the number of counts in the full energy peak (FEP), N_0 the number of target nuclei in the activation detector, ε^γ_{FEP} the absolute detection efficiency for the FEP, I_γ the intensity per decay, t_{irr} and t_{cool} the irradiation and cooling time, and t_{real} and t_{live} the real time and live time of the spectroscopic measurement. Corresponding corrections for gamma-ray attenuation in the activation foil and proton beam fluctuation are applied as well.

2.4. Neutron field determination

The neutron field of upgraded beryllium target station with the p(35)+Be source reaction in close source-to-sample distance was determined using the multi-foil activation method. At the NG-2 fast neutron generators, this experimental technique was formerly tested and successfully applied also for the neutron field measurement of the p(37)+D$_2$O source reaction with liquid target [14–16].

The set of eleven activation detectors (spectroscopy thin foils with diameter of 15 mm) for irradiation experiment consisted of Al, Au, In, Ti, Fe, Y, Lu, Co, Ni, Nb, and Bi. Activation materials were sensitive to various parts of the neutron energy spectrum according to the activation cross-sections. The irradiation experiment with the p+Be neutron source lasted for 13 hours, the proton beam current was reaching a value of 9.82 μA and energy of 35 MeV. The stacks of the foils were located on the aluminium holder in three beryllium-to-sample distances, in particular at a distance of 14 mm (position 0), 34 mm (position 2), and 154 mm (position 14). After irradiation, the induced radioactivity of activation foils was repeatedly measured by two semiconductor HPGe detectors after various cooling times. The reaction

Table 2. Activation reactions observed in irradiation experiment and used for neutron field reconstruction.

Reaction	E_{thresh} (MeV)	$T_{1/2}$	E_γ (keV)	I_γ (%)
^{27}Al(n,α)^{24}Na	3.25	14.96 h	1 368.63	100.00
^{nat}Ti(n,x)^{46}Sc	1.57	83.79 d	1 120.55	99.99
^{nat}Ti(n,x)^{47}Sc	0.00	3.35 d	159.78	68.30
^{nat}Ti(n,x)^{48}Sc	3.28	43.67 h	1 312.10	100.00
^{nat}Ti(n,x)^{47}Ca	3.33	4.54 d	1297.09	71.00
^{nat}Fe(n,x)^{51}Cr	0.00	27.70 d	320.08	10.00
^{nat}Fe(n,x)^{54}Mn	3.17	312.30 d	834.85	99.98
^{nat}Fe(n,x)^{56}Mn	2.87	2.58 h	846.77	98.90
^{59}Co(n,γ)^{60}Co	0.00	5.27 y	1 332.50	99.99
^{59}Co(n,2n)^{58}Co	10.51	70.86 d	810.78	99.00
^{59}Co(n,3n)^{57}Co	17.33	271.79 d	122.06	85.60
^{59}Co(n,p)^{59}Fe	1.49	44.50 d	1 099.25	56.50
^{59}Co(n,α)^{56}Mn	0.00	2.58 h	846.77	98.90
^{nat}Ni(n,x)^{60}Co	2.02	5.27 y	1 332.50	99.99
^{nat}Ni(n,x)^{58}Co	1.50	70.86 d	810.78	99.00
^{nat}Ni(n,x)^{57}Co	5.77	271.79 d	122.06	85.60
^{nat}Ni(n,x)^{57}Ni	12.21	35.60 h	1 377.63	81.70
^{89}Y(n,γ)^{90m}Y	0.00	3.19 h	202.51	97.30
^{89}Y(n,2n)^{88}Y	11.05	106.65 d	1 836.06	99.20
^{93}Nb(n,x)^{90m}Y	0.00	3.19 h	202.51	97.30
^{93}Nb(n,2n)^{92m}Nb	9.05	10.15 d	934.46	99.00
^{115}In(n,n′)^{115m}In	0.34	4.49 h	336.24	45.83
^{nat}Lu(n,x)^{176m}Lu	0.00	3.64 h	88.34	8.90
^{nat}Lu(n,x)^{173}Lu	14.19	1.37 y	78.63	11.87
^{197}Au(n,γ)^{198}Au	0.00	2.70 d	411.80	96.00
^{197}Au(n,2n)^{196}Au	8.19	6.18 d	355.68	87.00
^{197}Au(n,3n)^{195}Au	14.55	186.09 d	98.85	10.90
^{197}Au(n,4n)^{194}Au	23.21	38.02 h	293.55	10.40
^{209}Bi(n,3n)^{207}Bi	14.42	31.55 y	569.70	97.74

products observed in measured gamma-ray spectra were identified according to the energies, intensities, and half-life periods. Subsequently, the reaction rates were obtained and used for the neutron spectrum reconstruction. In total, thirty-three activation and thresholds reactions were observed in all foils.

3. Results

For neutron spectra reconstruction from measured reaction rates, the SAND-II unfolding code [17] was employed. Twenty-nine out of thirty-three experimental reaction rates (see Table 1) and the cross-sections from the EAF-2010 data library [18] were successfully used for neutron spectra reconstruction at three irradiation positions. As the initial guess neutron spectra for the SAND-II unfolding procedure, the MCNPX [19] predictions were utilized.
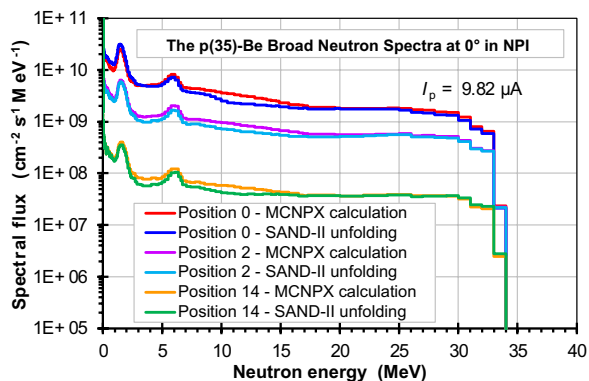
Figure 2. Neutron spectra of NG-2 generator at three irradiation positions measured by multi-foil activation technique at NPI.
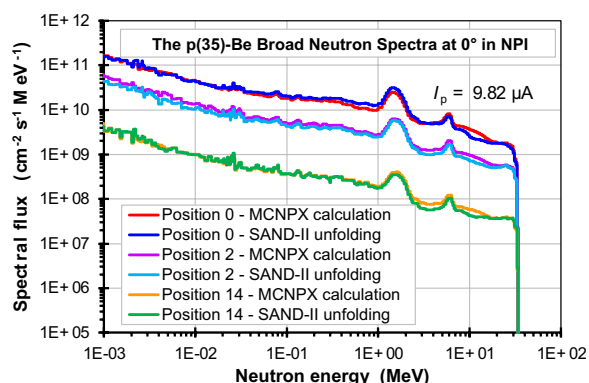

Figure 3. Neutron spectra of NG-2 generator at three irradiation positions displayed in log-log scale.
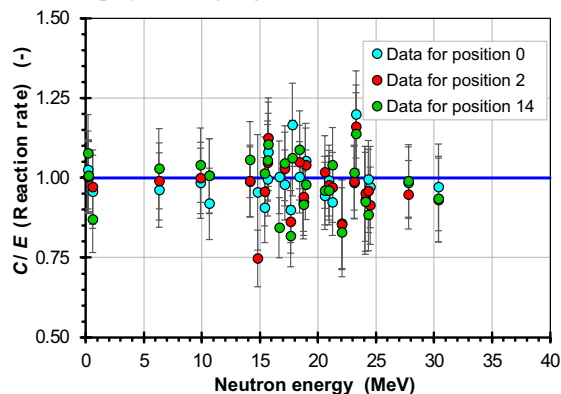

Figure 4. Calculated over experimental reaction rates ratios.

Figure 5. Reaction rates and spectral flux ratios for position 0 and position 2.

Figure 6. Reaction rates and spectral flux ratios for position 0 and position 14.

Figure 7. Reaction rates ratios in dependence on target-to-sample distance.

Newly obtained neutron spectra for rebuilt Be-target station at the NPI with the p(35)+Be source reaction are depicted in Fig. 1 in linear scale and in Fig. 2 in logarithmic energy scale. The SAND-II reconstructed spectra as well as the MCNPX predictions are displayed. The MCNPX calculations correspond well with spectra reconstructed from experimentally measured reaction rates. There is only small deviation in the region of 8 to 15 MeV probably due to space integration effect in the real activation foils. The corresponding *C/E* (calculated over experimental) reaction rates ratios are summarized in Table 2 for all three irradiation positions and reactions used in reconstructions; the graphical representation is given in Fig. 3. All *C/E* ratios are very close to unity, and it confirms the correctness of the SAND-II reconstructed spectra (at the 35 MeV energy region).
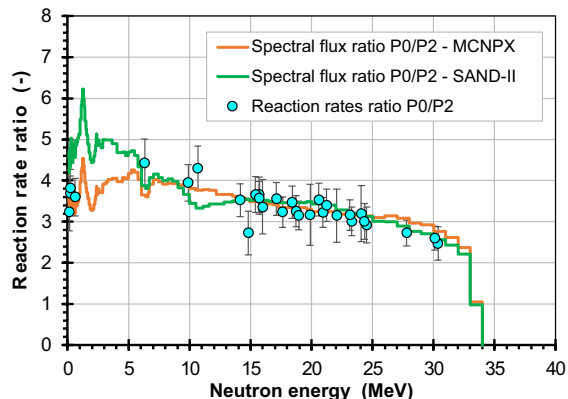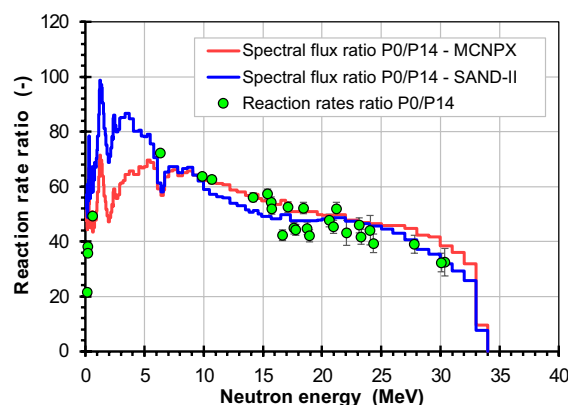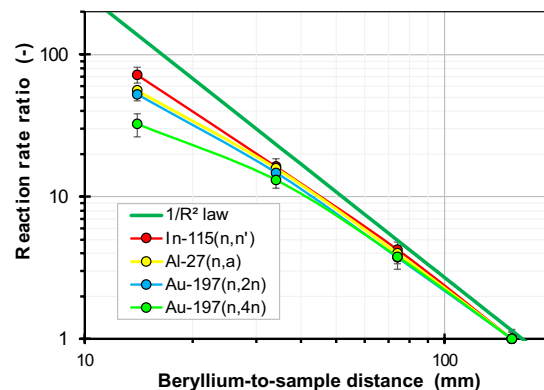
In Fig. 4, the ratios of experimental reaction rates of position 0 to position 2, the ratio of SAND-II unfolded spectra, and ratio of the MCNPX predictions for corresponding positions are depicted. The ratios of reaction rates, ratio of unfolded spectra as well as the ratio of MCNPX spectra are in good agreement, and they also confirm the correctness of the unfolded spectra. Small deviations between the SAND-II unfolding and MCNPX calculations are given by the space integration effect of neutron flux by the activation foils and forward orientation of the p+Be reaction. The same

Table 3. Calculated over experimental reaction rates ratios for adjusted neutron spectra.

Reaction	Position 0	Position 2	Position 14
^{27}Al(n,α)^{24}Na	0.99	0.99	1.06
^{nat}Ti(n,x)^{46}Sc	0.90	0.86	0.82
^{nat}Ti(n,x)^{47}Sc	1.20	1.16	1.14
^{nat}Ti(n,x)^{48}Sc	1.00	1.05	1.09
^{nat}Ti(n,x)^{47}Ca	0.86	0.85	0.83
^{nat}Fe(n,x)^{51}Cr	0.92	0.94	0.92
^{nat}Fe(n,x)^{54}Mn	1.05	1.04	0.98
^{nat}Fe(n,x)^{56}Mn	1.08	1.12	1.11
^{59}Co(n,γ)^{60}Co	1.02	1.00	1.08
^{59}Co(n,2n)^{58}Co	0.94	1.02	0.96
^{59}Co(n,3n)^{57}Co	0.98	0.95	0.99
^{59}Co(n,p)^{59}Fe	0.99	1.05	1.05
^{59}Co(n,α)^{56}Mn	0.91	0.96	1.01
^{nat}Ni(n,x)^{60}Co	0.95	0.75	–
^{nat}Ni(n,x)^{58}Co	0.98	1.00	1.04
^{nat}Ni(n,x)^{57}Co	0.92	0.97	1.04
^{nat}Ni(n,x)^{57}Ni	0.99	0.99	1.02
^{89}Y(n,γ)^{90m}Y	0.92	1.01	1.01
^{89}Y(n,2n)^{88}Y	0.99	0.98	0.96
^{93}Nb(n,x)^{90m}Y	1.00	–	0.84
^{93}Nb(n,2n)^{92m}Nb	1.17	–	1.06
^{115}In(n,n$'$)^{115m}In	0.96	0.99	1.03
^{nat}Lu(n,x)^{176m}Lu	0.96	0.97	0.87
^{nat}Lu(n,x)^{173}Lu	0.93	0.95	0.92
^{197}Au(n,γ)^{198}Au	1.01	1.00	1.01
^{197}Au(n,2n)^{196}Au	0.98	1.03	1.05
^{197}Au(n,3n)^{195}Au	0.97	0.91	–
^{197}Au(n,4n)^{194}Au	0.97	0.93	0.93
^{209}Bi(n,3n)^{207}Bi	0.99	0.96	0.88

comparison for position 0 to position 14 is performed in Fig. 5.

The reaction rate ratios (normalised to position 14) in dependence on beryllium-to-samples distance are displayed in Fig. 6; they show the deflection of rate values from $1/R^2$ law due to a non-point-like geometry of irradiation system and activation foils.

4. Conclusions

At the NPI, new neutron field based on the p(35)+Be reaction of upgraded Be-target station have been developed. The mean energy of obtained spectra is about 14.2 MeV, and it corresponds well with the equation proposed by M.A. Lone. The shape of neutron energy spectrum is in very good agreement with results from other authors, such as Brede [5], Howard [7], and Lone [3]. In experiment with a proton beam intensity of 9.82 μA, the fast neutron
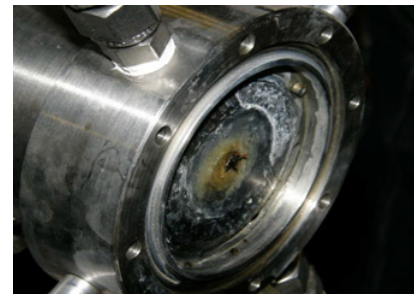

Figure 8. Open target station chamber with back side of Be target.

spectral flux reaches the value of 1.2×10^{11} cm^{-2}s^{-1} in position 0, 2.8×10^{10} cm^{-2}s^{-1} in position 2, and 2×10^9 cm^{-2}s^{-1} in position 14.

This neutron field represents a useful tool for integral benchmark experiments, integral validation of cross-sections for fusion related program IFMIF, testing the radiation hardness of electronics against the fast neutron fields, and for application of neutron activation analysis. Beside the knowledge of neutron field, the operational experience with Be-target was also obtained. In Fig. 7, there is an open target station chamber with the back side of Be-target, the blistering (swelling) effect caused by 35 MeV proton beam on the beryllium disc is evident.

References

[1] M. Winter, WebElements [Online] (August 2016), http://webelements.com
[2] National Nuclear Data Center, Q-value Calculator [Online] (September 2016), https://www.nndc.bnl.gov/qcalc
[3] M.A. Lone et al., Nucl. Instr. Meth. **143**, 331–344 (1977)
[4] R.G. Graves et al., Med. Phys. **6**, 123–128 (1970)
[5] H.J. Brede et al., Nucl. Instr. Meth. **274**, 332–344 (1989)
[6] S.W. Johnsen, Phys. Med. Biol. **23**, 499–502 (1978)
[7] W.B. Howard et al., Nucl. Sci. Eng. **138**, 145–160 (2001)
[8] F.M. Waterman et al., Med. Phys. **6**, 432–435 (1979)
[9] J.L. Ullman et al., Med. Phys. **8**, 396–397 (1981)
[10] S. Cierjacks, Neutron Source for Basic Physics and Applications (Oxford Pergamon Press, 1983)
[11] M. Stefanik et al., Nucl. Data Sheets **119**, 422–424 (2014)
[12] U. Mollendorf et al., "A nuclear simulation experiment for the International Fusion Materials Irradiation Facility (IFMIF) ", Karlsruhe (2002)
[13] M. Stefanik et al., Radiat. Phys. Chem. **104**, 302–305 (2014)
[14] S. Simakov et al., "Determination of Neutron Spectrum by the Dosimetry Foil Method up to 37 MeV", Reactor Dosimetry State of the Art 2008, Proceedings of the 13th International Symposium, Netherlands (2008)

[15] M. Stefanik et al., "The p-D_2O generator neutron spectrum determination by multi-foil activation method", Trans. ANS **106**, 894–896 (2012)

[16] M. Stefanik et al., "Accelerator driven p(37)-D_2O fast neutron Source at the NPI Rez", Proceedings of the 2014 15th International Scienti?c Conference on Electric Power Engineering, EPE 2014 (2014)

[17] SAND-II-SNL, PSR-345, UKAEA FUS (1996)

[18] R.A. Forrest et al., EAF-2010, UKAEA FUS (2010)

[19] L.S. Waters et al., MCNPX Users Manual V. 2.1.5